Science of the Total Environment 624 (2018) 1163–1170

Contents lists available at ScienceDirect

Science of the Total Environment

journal homepage: www.elsevier.com/locate/scitotenv

Simulations of summertime fossil fuel CO_2 in the Guanzhong basin, China

Tian Feng [a,b], Weijian Zhou [a,b,*], Shugang Wu [a,b], Zhenchuan Niu [a,b], Peng Cheng [a,b], Xiaohu Xiong [a,b], Guohui Li [a,c]

[a] State Key Laboratory of Loess and Quaternary Geology, Institute of Earth Environment, Chinese Academy of Sciences, Xi'an 710061, China
[b] Xi'an AMS Center, Xi'an 710061, China
[c] Key Laboratory of Aerosol Chemistry and Physics, Institute of Earth Environment, Chinese Academy of Sciences, Xi'an 710061, China

HIGHLIGHTS

- Recently added fossil fuel CO_2 presents a nocturnal peak and a rush-hour peak, associated with PBL and vehicle emission.
- Fossil fuel CO_2 in the basin is higher than the outside, reaching 40 ppmv in urban Xi'an and 15 ppmv in surrounding areas.
- Ignoring the influence of summer heterotrophic respiration in terrestrial biosphere would underestimate δCO_2ff by 0.38 ppmv.

GRAPHICAL ABSTRACT

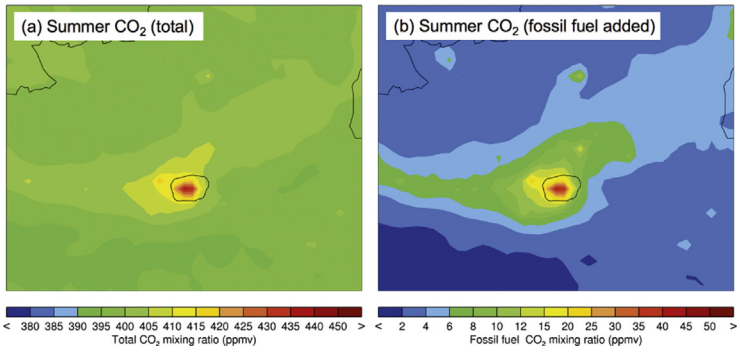

ARTICLE INFO

Article history:
Received 7 September 2017
Received in revised form 1 December 2017
Accepted 3 December 2017
Available online 27 December 2017

Editor: Jianmin Chen

Keywords:
$\Delta^{14}C$
Fossil fuel CO_2
WRF-CHEM
Guanzhong basin

ABSTRACT

Recent studies on fossil fuel CO_2 simulation associated with $\Delta^{14}CO_2$ measurements is quite limited, particularly in China. In this study, the fossil fuel CO_2 recently added to the atmosphere (δCO_2ff) over the Guanzhong basin, central China, during summer 2012 is simulated using a modified WRF-CHEM model constrained by measured CO_2 mixing ratio and $\Delta^{14}CO_2$. The model well captures the temporal variation of observed CO_2 mixing ratio and $\Delta^{14}CO_2$, and reasonably reproduces the distribution of observed $\Delta^{14}CO_2$. The simulation shows a significant variation of δCO_2ff during summertime, ranging from <5 ppmv to ~100 ppmv and no remarkable trend of δCO_2ff is found for June, July, and August. The δCO_2ff level is closely associated with atmospheric diffusion conditions. The diurnal cycle of δCO_2ff presents a double-peak pattern, a nocturnal one and a rush-hour one, related to the development of planetary boundary layer and CO_2 emission from vehicles. The spatial distributions of summertime δCO_2ff within the basin is clearly higher than the outside, reaching up to 40 ppmv in urban Xi'an and 15 ppmv in its surrounding areas, indicative of large local fossil fuel emissions. Furthermore, we find that neglecting the influence of summer heterotrophic respiration in terrestrial biosphere would slightly underestimate the calculated δCO_2ff by about 0.38 ppmv in the basin.

1. Introduction

Since the industrial revolution, fossil fuel-derived carbon dioxide (CO_2ff) has largely contributed to atmospheric carbon dioxide (CO_2) (Stocker et al., 2013) and resulted in a continuous increase of atmospheric CO_2 mole fraction, which is closely related to global warming

* Corresponding author at: State Key Laboratory of Loess and Quaternary Geology, Institute of Earth Environment, Chinese Academy of Sciences, Xi'an 710061, China.
E-mail address: weijian@loess.llqg.ac.cn (W. Zhou).

https://doi.org/10.1016/j.scitotenv.2017.12.021
0048-9697/

and climate change (Stocker et al., 2013). Le Quéré et al. (2016) have assessed that global CO_2 emissions from fossil fuels is about 9.3 GtC yr^{-1} during last decade (2006–2015), with an average growth of 1.8% per year. This amount accounts for 91% of the total CO_2 emissions and contributes largely to the global carbon budget during the decade (Le Quéré et al., 2016).

Traditionally, CO_2ff emission is obtained using the "bottom-up" approach, in which CO_2ff is estimated based on fossil fuel consumption and a series of coefficients and scaling factors in each sector. This approach potentially involves large uncertainties (Marland et al., 2009). For example, Marland et al. (2009) have reported that the estimated CO_2ff likely has an uncertainty of 3–40% at national and annual scale and varies widely in country and method. Compared with the traditional approach, radiocarbon content of CO_2 ($\Delta^{14}CO_2$) provides a more scientific and effective method to isolate the recently added CO_2ff (Levin et al., 1989). Radiocarbon (^{14}C), naturally produced in the atmosphere by cosmic-ray neutron interactions with nitrogen nuclei, has a radioactive half-life of 5730 years (Godwin, 1962). Once produced, ^{14}C is rapidly oxidized to $^{14}CO_2$ and distributed around the globe. $\Delta^{14}C$ denotes the per mil (‰) deviation of ^{14}C content from a standard material, corrected for isotopic fractionation and radioactive decay since the time of collection (Stuiver and Polach, 1977). Given the observed (Δ_{obs}) and background (Δ_{bkg}) $\Delta^{14}C$ and the observed CO_2 mixing ratio, the recently added CO_2ff (δCO_2ff) is determined using the following equation (Turnbull et al., 2009):

$$\delta CO_2 ff = \frac{CO_2 obs(\Delta_{obs} - \Delta_{bkg})}{\Delta_{ff} - \Delta_{bkg}} - \frac{CO_2 oth(\Delta_{oth} - \Delta_{bkg})}{\Delta_{ff} - \Delta_{bkg}} \quad (1)$$

where Δ_{ff} is the $\Delta^{14}C$ value of CO_2ff, which equals −1000‰ since fossil fuel is buried much longer than the half-life of ^{14}C. The second term of the equation, $\beta = \frac{CO_2 oth(\Delta_{oth} - \Delta_{bkg})}{\Delta_{ff} - \Delta_{bkg}}$, is a small correction for ^{14}C from other small sources, primarily heterotrophic respiration of terrestrial biosphere in inland regions (Miller et al., 2012; Turnbull et al., 2009; 2006).

With the rapid increase in economy during recent decades, China has been consuming an increasing amount of fossil fuel, injecting a large amount of CO_2 into the atmosphere (Gregg et al., 2008). Le Quéré et al. (2016) have reported that China is the largest contributor to global CO_2 emission in 2015 and accounts for 29% (2.87 GgC) of the total CO_2 emission. The estimation of CO_2 emission in China could be quite uncertain. For example, Gregg et al. (2008) have reported that the uncertainty in Chinese emission is about ±10%. Liu et al. (2015) have even found that the CO_2 emission in China during 2000–2013 are overestimated by 2.9 GgC which is larger than the total forest sink during 1990–2007 (2.66 GgC) or the land carbon sink during 2000–2009 (2.6 GgC) in China. This large uncertainty poses a great challenge in the development of CO_2 control policies for China.

During recent years, the advanced $\Delta^{14}C$ method has been adopted, although quite limited, in China's fossil fuel CO_2 observations. For example, Zhou et al. (2014) used $\Delta^{14}C$ to trace fossil fuel CO_2 in Xi'an City, China. Niu et al. (2016b) measured atmospheric $\Delta^{14}CO_2$ during 2014 in Beijing and Xiamen, China. The calculated δCO_2ff in Beijing and Xiamen are 39.7 and 13.6 ppm, respectively, averaged over 2014 and significant seasonal variations of δCO_2ff are found in both cities. Niu et al. (2016a) measured the $\Delta^{14}CO_2$ at a global background site (Waliguan) and three regional background sites in China and highlighted that the $\Delta^{14}CO_2$ at regional background sites is significantly lower than those at the global background site. So far, the reported $\Delta^{14}CO_2$ studies in China are confined to scarce ground-based measurements.

The simulations of δCO_2ff using atmospheric models have been performed. For example, Rivier et al. (2006) used a chemistry transport model to evaluate the relationship between δCO_2ff and SF_6, C_2Cl_4, and CO in the Northern Hemisphere, and recommended the use of C_2Cl_4 as a proxy of δCO_2ff. Gamnitzer et al. (2006) simulated δCO_2ff in Europe using a regional transport model to investigate the application of CO as a quantitative tracer for δCO_2ff. Liu et al. (2017) simulated the spatiotemporal patterns of δCO_2ff in central Europe using a high-resolution atmospheric transport model. However, very limited studies have been performed to simulate δCO_2ff in association with $\Delta^{14}CO_2$ observations (e.g., Turnbull et al., 2009, 2016). To the best of our knowledge, the modeling studies of δCO_2ff constrained by $\Delta^{14}CO_2$ measurements have not been reported in China.

In this study, we simulate atmospheric CO_2 in association with $\Delta^{14}CO_2$ measurements during summertime in the Guanzhong basin,

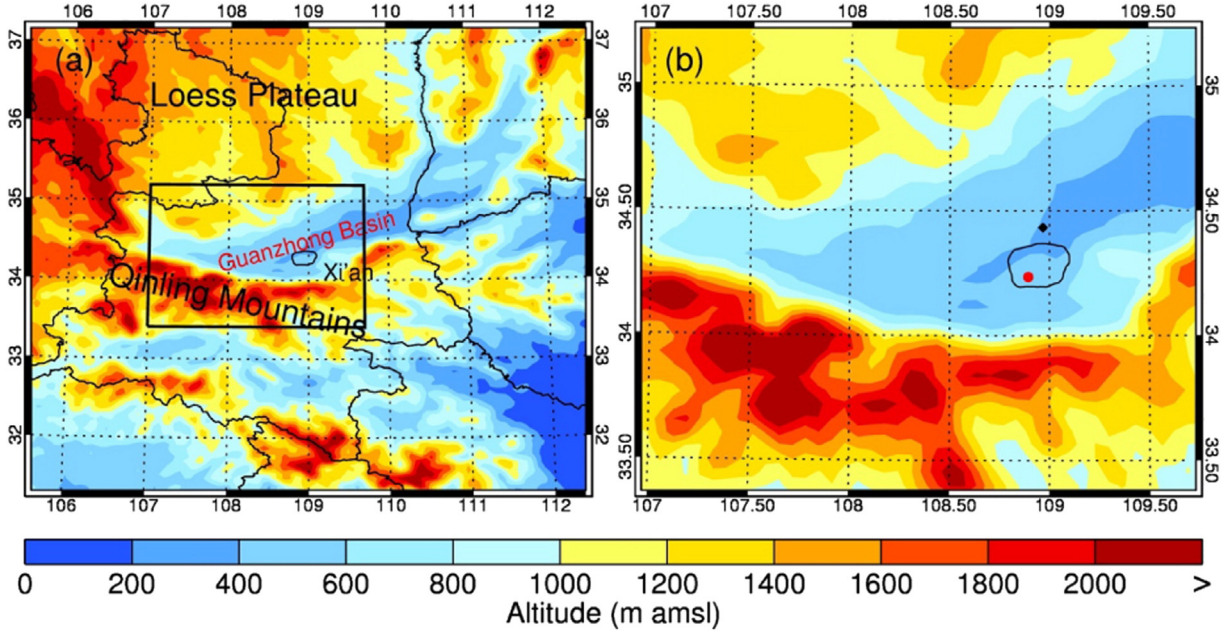

Fig. 1. Map showing (a) the simulation domain, and (b) the topography of the Guanzhong basin. The red spot shows the location of Institute of Earth Environment, Chinese Academy of Sciences (IEECAS). The black diamond presents the location of the Jinghe meteorological station.

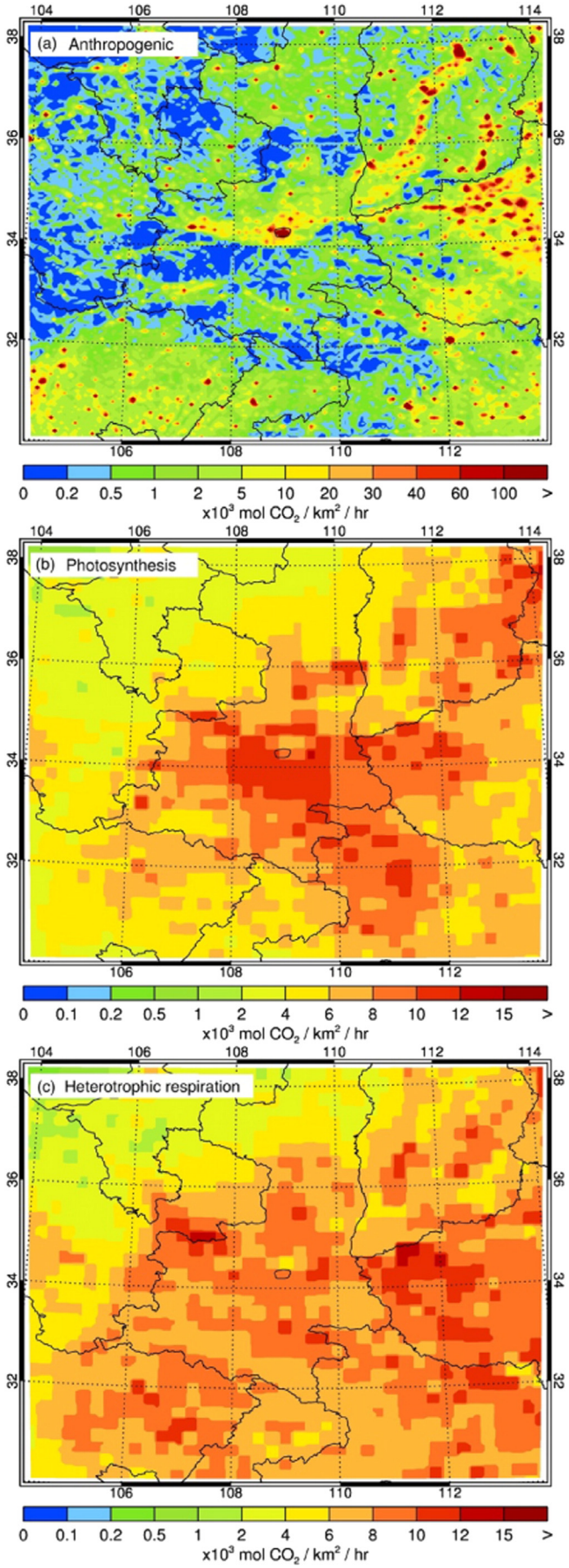

Fig. 2. Geographic distributions of (a) anthropogenic CO_2 emissions and (b) absorbed CO_2 in photosynthesis and (c) exhalant CO_2 in heterotrophic respiration of terrestrial biosphere in the simulation domain. The black curves present provincial boundaries in China and the location of Xi'an.

an area in central China with rapid industrialization and urbanization, using the Weather Research and Forecasting model coupled with atmospheric chemistry (WRF-CHEM). The objectives of this study are to preliminarily investigate the temporal variability and spatial distributions of summertime δCO_2ff in the basin. We describe the model and its configuration in Section 2. The results of model simulations and comparisons are given in Section 3 and the main conclusions are summarized in Section 4.

2. Model and methods

2.1. WRF-CHEM model

A revised version of the WRF-CHEM model, based on the official version 3.8.1, is applied to simulate the summertime atmospheric CO_2 in the Guanzhong basin, China. This specific version includes the CO_2 exchange of terrestrial vegetation with the atmosphere, which is treated as follows:

$$CO_2\mathrm{tot}(t) = CO_2\mathrm{bkg}(t) + \delta CO_2\mathrm{ff}(t) + \delta CO_2\mathrm{oth}(t) \tag{2}$$

$$CO_2\mathrm{bkg}(t+1) = CO_2\mathrm{bkg}(t) + [CO_2Rh(t+1) - CO_2NPP(t+1)] \times \frac{CO_2\mathrm{bkg}(t)}{CO_2\mathrm{tot}(t)} \tag{3}$$

$$\delta CO_2\mathrm{ff}(t+1) = \delta CO_2\mathrm{ff}(t) + [CO_2Rh(t+1) - CO_2NPP(t+1)] \times \frac{\delta CO_2\mathrm{ff}(t)}{CO_2\mathrm{tot}(t)} \tag{4}$$

$$\delta CO_2\mathrm{oth}(t+1) = \delta CO_2\mathrm{oth}(t) + [CO_2\mathrm{Rh}(t+1) - CO_2\mathrm{NPP}(t+1)] \times \frac{\delta CO_2\mathrm{oth}(t)}{CO_2\mathrm{tot}(t)} \tag{5}$$

Atmospheric CO_2 is divided into 3 categories: background CO_2 (CO_2bkg), recently added fossil fuel CO_2 (δCO_2ff), and other recently added CO_2 (δCO_2oth, mainly from terrestrial biosphere (Turnbull et al., 2009); CO_2tot is the total of these 3 categories. CO_2Rh and CO_2NPP denote CO_2 emission in heterotrophic respiration and absorption in photosynthesis of the terrestrial biosphere. The dry deposition of CO_2 is parameterized following Wesely (1989) and the wet scavenging of CO_2 is switched off in this study.

The derivation of $\Delta^{14}CO_2$ in the model is calculated following below:

$$CO_2\mathrm{tot} = CO_2\mathrm{bkg} + \delta CO_2\mathrm{ff} + \delta CO_2\mathrm{oth} \tag{6}$$

$$\Delta_{\mathrm{tot}} \cdot CO_2\mathrm{tot} = \Delta_{\mathrm{bkg}} \cdot CO_2\mathrm{bkg} + \Delta_{\mathrm{ff}} \cdot \delta CO_2\mathrm{ff} + \Delta_{\mathrm{oth}} \cdot \delta CO_2\mathrm{oth} \tag{7}$$

Given Δ_{bkg}, Δ_{ff}, and Δ_{oth}, Δ_{tot} is calculated as

$$\Delta_{\mathrm{tot}} = \frac{\Delta_{\mathrm{bkg}} \cdot CO_2\mathrm{bkg} + \Delta_{\mathrm{ff}} \cdot \delta CO_2\mathrm{ff} + \Delta_{\mathrm{oth}} \cdot \delta CO_2\mathrm{oth}}{CO_2\mathrm{bkg} + \delta CO_2\mathrm{ff} + \delta CO_2\mathrm{oth}} \tag{8}$$

Turnbull et al. (2009) have reported that heterotrophic respiration in terrestrial biosphere is expected to be the main contributor to Δ_{tot} for land regions. Therefore, we use Δ_{hr} instead of Δ_{oth} to estimate modeled Δ_{tot}:

$$\Delta_{\mathrm{tot}} = \frac{\Delta_{\mathrm{bkg}} \cdot CO_2\mathrm{bkg} + \Delta_{\mathrm{ff}} \cdot \delta CO_2\mathrm{ff} + \Delta_{\mathrm{hr}} \cdot \delta CO_2\mathrm{hr}}{CO_2\mathrm{bkg} + \delta CO_2\mathrm{ff} + \delta CO_2\mathrm{hr}} \tag{9}$$

where $\Delta_{\mathrm{ff}} = -1000‰$ and Δ_{bkg} uses the monthly mean of measured $\Delta^{14}CO_2$ at the Jungfraujoch global background station. Turnbull et al.

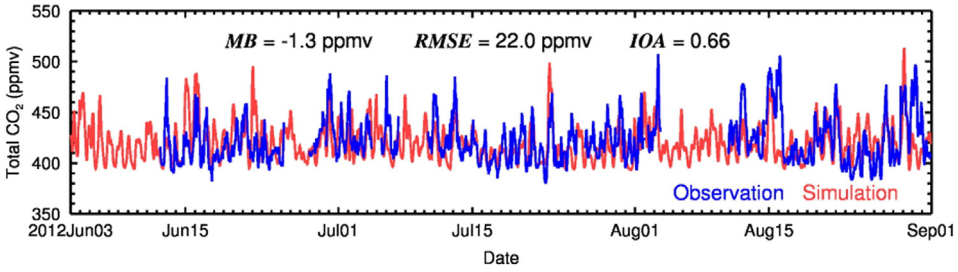

Fig. 3. Temporal variations of simulated (red curve) and observed (blue curves) total CO_2 mixing ratio at IEECAS, Xi'an.

(2006) have estimated $\Delta_{hr} = 166 \pm 100‰$ in terrestrial biosphere of the Northern Hemisphere. This value varies quite widely and our assessment of $\Delta_{hr} = 66‰$ in the Guanzhong basin results in the best fitted Δ_{tot} with the observation (see below).

2.2. Model configuration

We simulate summertime atmospheric CO_2 concentration from 1 June to 31 August 2012 in the Guanzhogn basin, China. The WRF-CHEM model is configured with grid spacing of 6 km (150 × 150 grid points) and centered at 109°E and 34.25°N (Fig. 1). Thirty-five stretched vertical levels with spacing ranging from 50 m near the surface to 500 m at 2.5 km a.g.l and >1 km above 14 km are adopted in the configuration. The model employs the microphysics of Lin et al. (1983), the Mellor-Yamada-Janjic (MYJ) turbulent kinetic energy (TKE) planetary boundary layer (PBL) scheme and the MYJ surface layer scheme (Janjić, 2002), the Unified Noah land-surface model (Chen and Dudhia, 2001), and the New Goddard shortwave (Chou and Suarez, 1999) and longwave (Chou et al., 2001) schemes. Meteorological initial and boundary conditions are obtained from NCEP 1° × 1° reanalysis data. The chemical initial and boundary conditions of CO_2 are interpolated from the s04_v3.8 run with a 6-h interval of Jena CarboScope (http://www.bgc-jena.mpg.de/~christian.roedenbeck/download-CO2/). The spin-up time of the model is 1 day.

The employed anthropogenic CO_2 inventory from fossil fuel combustion is developed by Zhang et al. (2009), which includes contributions from agriculture, industry, power generation, and residential and transportation sources (Fig. 2). The CO_2 flux of terrestrial biosphere represented as respired and photosynthetic CO_2 is interpolated from the monthly data of Global Fire Emissions Database, Version 4 (GFEDv4, https://doi.org/10.3334/ORNLDAAC/1293).

2.3. Observations

We use the Picarro G2131-i isotopic-CO_2 gas analyzer (Picarro Inc., Santa Clara, CA, USA) to measure hourly CO_2 mixing ratio at IEECAS, Xi'an (Fig. 1) online. The CO_2 detection line of this analyzer is 0.1 ppmv. The sampling method of a displacement of phosphoric acid solution is used to measure daily/multi-day CO_2 mixing ratio and to derive atmospheric $\Delta^{14}CO_2$ at IEECAS, Xi'an (108.89°E, 34.23°N, Fig. 1b). This method has been employed in a previous study and proved reliable (Zhou et al., 2014). Upper maize leaves growing in summer are collected and sampled to present summertime $\Delta^{14}CO_2$ in the basin.

2.4. Statistics

In this study, the mean bias (MB), the root mean square error (RMSE), and the index of agreement (IOA) are used to evaluate the WRF-CHEM model simulations of ground CO_2 concentrations and $\Delta^{14}CO_2$.

$$MB = \frac{1}{N}\sum_{i=1}^{N}(P_i - O_i) \tag{10}$$

$$RMSE = \left[\frac{1}{N}\sum_{i=1}^{N}(P_i - O_i)\right]^{\frac{1}{2}} \tag{11}$$

$$IOA = 1 - \frac{\sum_{i=1}^{N}(P_i - O_i)}{\sum_{i=1}^{N}\left(|P_i - \overline{O}| + |O_i - \overline{O}|\right)} \tag{12}$$

where P_i and O_i denote the simulated and observed variables, respectively. N is the total number of predictions and $\overline{O}$ is the average of observations. Dimensionless IOA has a theoretical range from 0 to 1, with a value of 1 suggesting perfect agreement between simulation and observation.

3. Results and discussion

3.1. Model performance

The model performance is validated using the online hourly observation of CO_2 mixing ratio and daily (or multi-day) CO_2 and $\Delta^{14}CO_2$ at IEECAS, Xi'an, and $\Delta^{14}CO_2$ from maize leaves in the basin.

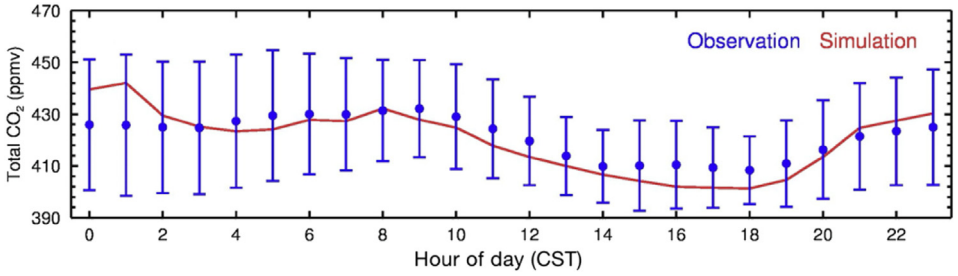

Fig. 4. Diurnal cycle of simulated (red curve) and observed (blue error bars) total CO_2 mixing ratio at IEECAS, Xi'an averaged over June, July, and August. Blue bars show the standard deviation of observed CO_2 mixing ratio during summertime.

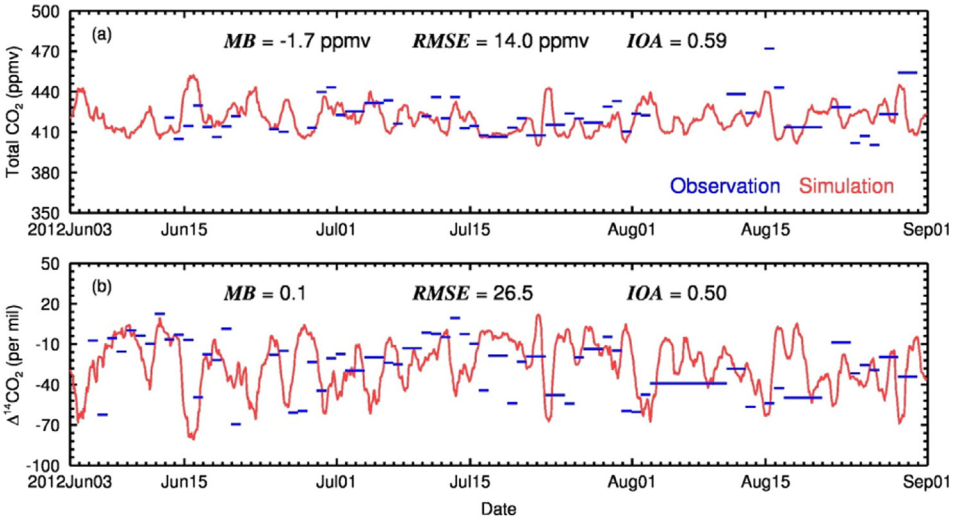

Fig. 5. Temporal variations of simulated (red curve) and observed (blue bars) (a) total CO_2 concentration and (b) $\Delta^{14}CO_2$ at IEECAS, Xi'an.

3.1.1. Temporal variability of CO_2 mixing ratio and $\Delta^{14}CO_2$

Fig. 3 presents the temporal variation of estimated CO_2 mixing ratio from June to August 2012 at IEECAS, Xi'an against the hourly CO_2 observations. The observed CO_2 profile shows that the CO_2 mixing ratio is generally >400 ppmv at IEECAS during summertime with peak values higher than 500 ppmv. The model reasonably reproduces the variations, despite some discrepancies. No obvious CO_2 trend is found from the observation or simulation during the 3 months. Statistics on the simulated and observed CO_2 shows that MB and RMSE are −1.3 ppmv and 22.0 ppmv, respectively, and IOA reaches 0.66.

The simulated diurnal cycle of CO_2 mixing ratio averaged over summertime is compared with the observation and specifically presented in Fig. 4. The observation shows that the mean CO_2 mixing ratio in summer is about 425 ppmv with a clear diurnal cycle. The observed nocturnal CO_2 mixing ratio is higher than that during daytime, showing a profound effect of the diurnal variation of planetary boundary layer height.

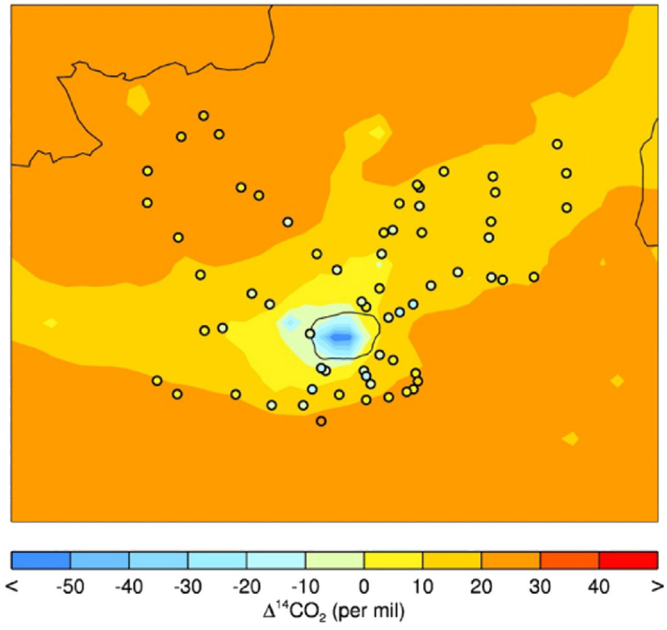

Fig. 6. Spatial distributions of simulated $\Delta^{14}CO_2$ (colored contours) compared with observed $\Delta^{14}CO_2$ from maize leaves (colored spots) in the basin.

It is worth noting that the higher CO_2 mixing ratio at about 08:00 a.m. (local time, LT), i.e. morning rush hours, strongly points to the influence of transportation emission. As a comparison, the model well reproduces the observed diurnal cycle of summertime CO_2 mixing ratio, although with a larger variability. The simulation slightly underestimates the daytime CO_2 mixing ratio and overestimates the nocturnal one, particularly at mid-night; while the deviation is much less than the standard deviation of observation.

The simulated temporal variations of atmospheric CO_2 mixing ratio and $\Delta^{14}CO_2$ are further validated against the observations obtained from the displacement of phosphoric acid solution (Fig. 5). Horizontal bars in the figure show the durations of measurements. Model results are smoothed over 24 h. Fig. 5a shows that the model well captures measured atmospheric CO_2 levels, ranging from ~400 to ~460 ppmv. Statistics on the simulation and measurement shows that the MB and RMSE are −1.7 ppmv and 14.0 ppmv, respectively, and the IOA is 0.59. The measured daily/multi-day $\Delta^{14}CO_2$ at IEECAS, Xi'an varies from ~15 to ~ − 70; the range is reasonably reproduced by the model with a MB of 0.1. The coincidence of the simulated high CO_2 mixing ratio and low $\Delta^{14}CO_2$ strongly suggests the important role of fossil fuel CO_2 during high CO_2 episodes. We note that the IOAs are relatively low, indicating the difficulty in replicating the variabilities of CO_2 and $\Delta^{14}CO_2$ observations. These biases are probably owing to the uncertainties in CO_2 emission and the simulated meteorological fields which is interpolated from coarse (1° × 1°) reanalysis data.

3.1.2. Spatial distribution of $\Delta^{14}CO_2$

Maize leaves, as an alternative of atmospheric $\Delta^{14}CO_2$ signature, are often used to represent atmospheric $\Delta^{14}CO_2$ during its growth period (Bozhinova et al., 2016). In northern China, maize grows in the summer season (Wang et al., 2014). The simulated spatial distribution of summertime $\Delta^{14}CO_2$ is shown in Fig. 6 along with the measurements from maize leaves in the basin. The spatial pattern of measured $\Delta^{14}CO_2$ presents lower values inside the basin and higher on the edge and outside of the basin, showing more fossil fuel CO_2 emission in the basin. This spatial pattern is replicated by the model, in which $\Delta^{14}CO_2$ show a clear boundary between the inside and outside of the basin. Outside of the basin, $\Delta^{14}CO_2$ is higher than 20; while for inside of the basin, $\Delta^{14}CO_2$ is lower. $\Delta^{14}CO_2$ in urban areas, offset by more fossil fuel combustion, is lower than that in non-urban areas. This is obvious in Xi'an, where $\Delta^{14}CO_2$ is lower than −50. Although the model reasonably reproduces the observed $\Delta^{14}CO_2$ levels derived from maize leaves, the overestimation of $\Delta^{14}CO_2$ by the model is not ignorable. It should be

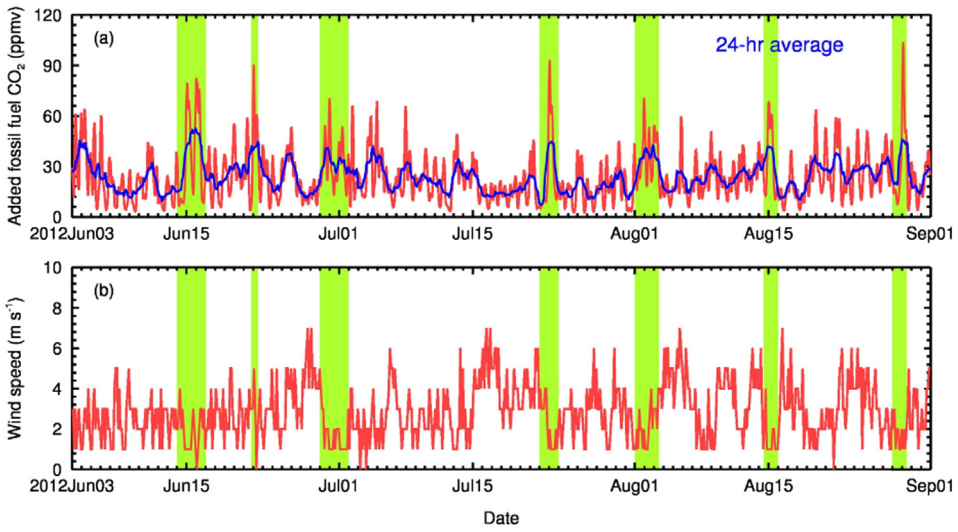

Fig. 7. Temporal variations of (a) simulated added fossil fuel CO_2 concentration at IEECAS, Xi'an and (b) observed wind speed at the Jinghe meteorological station. The blue curve in (a) shows the 24-h average of hourly δCO_2ff mixing ratio. Green shades present typical high δCO_2ff episodes along with low wind speed.

noted that the maize samples are obtained along the roads, potentially influenced by the traffic emissions, and hence the $\Delta^{14}CO_2$ tends to be lower, which cannot be well presented in the model. In addition, more information of the growing period of maize in the basin is needed in future to more precisely compare the simulated and maize leaf-derived $\Delta^{14}CO_2$.

The above comparison between model result and measurement reveals a reasonable model simulation of temporal variation and spatial distribution of CO_2 mixing ratio and $\Delta^{14}CO_2$ in the basin, suggesting that the employed CO_2 emission inventories are rational and the WRF-CHEM model is reliable to simulate the temporal variability and spatial pattern of fossil fuel CO_2 in the basin.

3.2. Temporal variability of δCO_2ff

Fig. 7a shows the simulated temporal variation of δCO_2ff mixing ratio at IEECAS, Xi'an from June to August 2012. δCO_2ff varies largely from <5 to ~100 ppmv at peak time with an average of 24.1 ppmv. The 24-h average δCO_2ff mixing ratio shows that daily δCO_2ff at IEECAS ranges from 10 to 55 ppmv in summer. Although the calculation shows that δCO_2ff in July (21.2 ppmv) is lower than that in June (25.4 ppmv) and August (25.8 ppmv), no remarkable trend is presented by the 24-h average δCO_2ff during the 3 months in Fig. 7a. The temporal variation of surface wind speeds at the Jinghe meteorological station in Fig. 7b implies a close relationship between δCO_2ff mixing ratio and the intensity of atmospheric dispersion. High (low) δCO_2ff mixing ratio episodes often correspond with low (high) wind speeds, which indicates that the δCO_2ff in the basin is easily built up when the air is stagnant and a strong air dispersion with high wind speed can result in a relatively low δCO_2ff mixing ratio.

The diurnal cycle of δCO_2ff mixing ratio at IEECAS is shown in Fig. 8. The temporal profile of δCO_2ff within a day presents a double-peak pattern, a peak at night and another at 08:00 a.m. (LT). Similar to the diurnal cycle of $\Delta^{14}CO_2$, these 2 peaks are explained by the low nocturnal PBL height and the abundant traffic emissions during morning rush hours, respectively. The δCO_2ff mixing ratio exceeds 30 ppmv during these 2 periods averaged over the entire summer and is diluted to ~12 ppmv by the elevated PBL in the afternoon.

3.3. Spatial distribution of δCO_2ff

The spatial distributions of CO_2 and δCO_2ff mixing ratio in the basin from June to August 2012 are shown in Fig. 9. The CO_2 mixing ratio outside the basin, treated as the CO_2 background of the basin, is about 390–400 ppmv. The lowest regional CO_2 background is over the Qinling Mountains, where the abundant terrestrial vegetation absorbs a large amount of atmospheric CO_2. Similarly, the δCO_2ff mixing ratio outside of the basin is generally quite low, <4 ppmv, which agrees well with the distribution of residents and anthropogenic CO_2 emissions. In contrast, the CO_2 and δCO_2ff mixing ratios in the basin, especially in the urban areas, are apparently higher than the outside. Fig. 9 shows that the raised CO_2 mixing ratio in the basin is almost attributed to the fossil fuel source. The rise of CO_2 mixing ratio compared to the background reaches up to 40 ppmv in urban Xi'an and about 15 ppmv in its surrounding areas, in good agreement with δCO_2ff mixing ratio.

3.4. δCO_2ff offset by terrestrial biosphere

Turnbull et al. (2009) have reported that neglecting the bias in heterotrophic respiration of terrestrial biosphere can lead to an

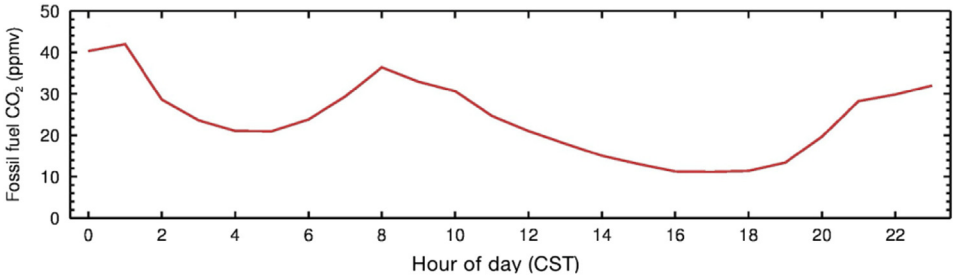

Fig. 8. Diurnal cycle of simulated added fossil fuel CO_2 concentration at IEECAS, Xi'an.

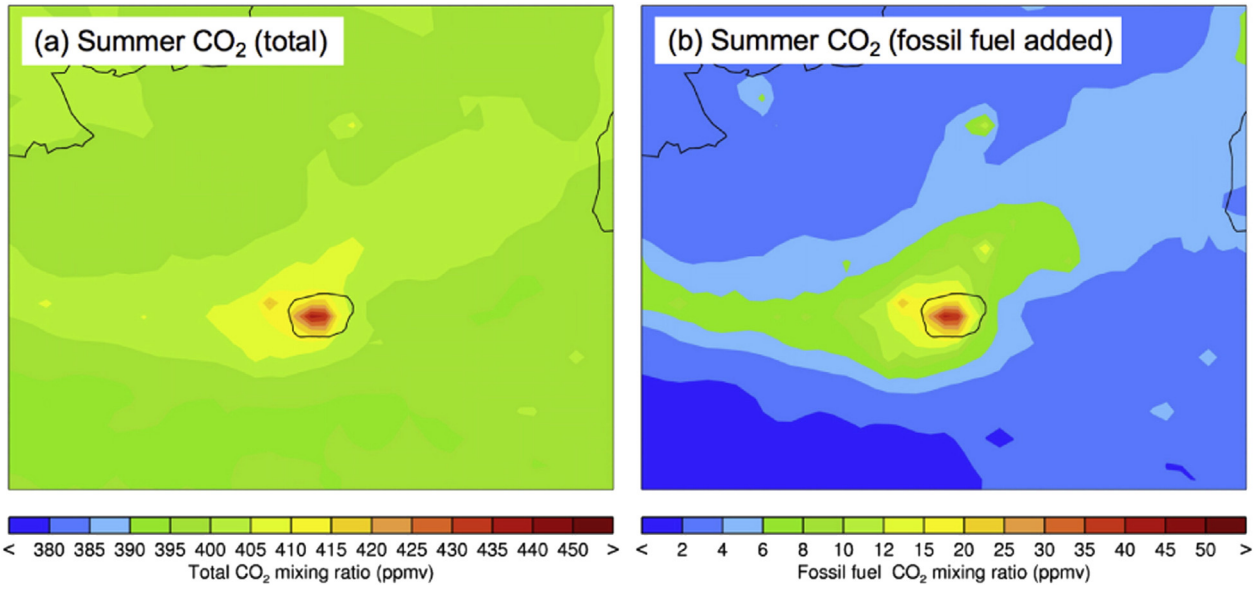

Fig. 9. Spatial distributions of simulated (a) CO_2 and (b) δCO_2ff mixing ratios in the basin.

underestimation of fossil fuel CO_2, typically 0.2–0.5 ppmv with a maximum in summer. However, the bias in fossil fuel CO_2 over Xi'an has never been assessed. Here, we estimate the impact of heterotrophic respiration on the derivation of recently added fossil fuel CO_2 by assuming $\Delta_{oth} = \Delta_{bkg}$ in Eq. (1). When employing this approximation, we obtain a fossil fuel CO_2 mixing ratio of 22.18 ppmv averaged over summertime 2012 within Xi'an, 0.38 ppmv less than the level with heterotrophic respiration of terrestrial biosphere considered. This result suggests that the recently added fossil fuel CO_2 in inland cities of China is probably underestimated slightly by the traditional approximated equation.

4. Conclusions

In this study, the summertime fossil fuel CO_2 recently added to the atmosphere is simulated using a modified WRF-CHEM model. The measurements of CO_2 mixing ratio in different time resolution and derived $\Delta^{14}CO_2$ using AMS are used to constrain the model simulation. The model reasonably simulates the observed temporal variation of CO_2 mixing ratio and well captures the diurnal variation at IEECAS, Xi'an. The measured $\Delta^{14}CO_2$ variation is reasonably reproduced by the model. The simulated spatial pattern of summertime $\Delta^{14}CO_2$ within the basin is evidently lower than that outside the basin, which is in accordance with the $\Delta^{14}CO_2$ measurements from maize leaves growing in summer. The reasonable performance of the WRF-CHEM model in simulating summertime CO_2 mixing ratio in Xi'an and $\Delta^{14}CO_2$ in the basin indicates that it is reliable to estimate recently added fossil fuel CO_2 in the basin using the current model and configuration.

The temporal variation of simulated δCO_2ff in summer 2012 is analyzed. The variation of δCO_2ff mixing ratio is dramatic, ranging from <5 to ~100 ppmv, and the daily δCO_2ff varies from 10 to 55 ppmv. No remarkable trend of δCO_2ff is found during June – August 2012. The relationship between δCO_2ff mixing ratio and wind speeds suggests an anti-correlation between δCO_2ff and the intensity of atmospheric dispersion, that is, high (low) δCO_2ff episodes often correspond with low (high) wind speeds. The diurnal variation of δCO_2ff presents a double-peak pattern, a nocturnal and rush-hour peak, which is closely related with the development of PBL and CO_2 emission from vehicles. The spatial distributions of summertime CO_2 and δCO_2ff mixing ratio in the basin is much higher than the outside, especially in the urban areas. The CO_2 mixing ratio elevated by local fossil fuel sources reaches up to 40 ppmv in urban Xi'an and about 15 ppmv in its surrounding areas.

Neglecting the influence of heterotrophic respiration in terrestrial biosphere in the basin can lead to an underestimation of δCO_2ff by about 0.38 ppmv in summer. This small underestimation shows that the approximation of the typical method (Eq. 1) has a minor effect on δCO_2ff calculation in inland cities of China.

Acknowledgments

This work was jointly supported by the 61st China Postdoctoral Science Foundation (No. 2017M613236) and National Natural Science Foundation of China (No. 41730108).

References

Bozhinova, D., Palstra, S.W.L., van der Molen, M.K., Krol, M.C., Meijer, H.A.J., Peters, W., 2016. Three years of Δ14CO2 observations from maize leaves in the Netherlands and Western Europe. Radiocarbon 58:459–478. https://doi.org/10.1017/rdc.2016.20.

Chen, F., Dudhia, J., 2001. Coupling an advanced land surface-hydrology model with the Penn State-NCAR MM5 modeling system. Part II: Preliminary model validation. Mon. Weather Rev. 129:569–585. https://doi.org/10.1175/1520-0493(2001)129<0569:caalsh>2.0.co;2.

Chou, M.-D., Suarez, M.J., 1999. A solar radiation parameterization for atmospheric studies (No. NASA/TM-1999- 10460). NASA Technique Report.

Chou, M.-D., Suarez, M.J., Liang, X.-Z., Yan, M.M.H., 2001. A thermal infrared radiation parameterization for atmospheric studies (No. NASA/TM-2001-104606). NASA Technique Report.

Gamnitzer, U., Karstens, U., Kromer, B., Neubert, R.E.M., Meijer, H.A.J., Schroeder, H., Levin, I., 2006. Carbon monoxide: A quantitative tracer for fossil fuel CO2? J. Geophys. Res. 111. https://doi.org/10.1029/2005jd006966.

Godwin, H., 1962. Half-life of radiocarbon. Nature 195:984. https://doi.org/10.1038/195984a0.

Gregg, J.S., Andres, R.J., Marland, G., 2008. China: emissions pattern of the world leader in CO2 emissions from fossil fuel consumption and cement production. Geophys. Res. Lett. 35:7663. https://doi.org/10.1029/2007GL032887.

Janjić, Z.I., 2002. Nonsingular implementation of the Mellor–Yamada level 2.5 scheme in the NCEP Meso model. NCEP Office Note.

Le Quéré, C., Andrew, R.M., Canadell, J.G., Sitch, S., Korsbakken, J.I., Peters, G.P., Manning, A.C., Boden, T.A., Tans, P.P., Houghton, R.A., Keeling, R.F., Alin, S., Andrews, O.D., Anthoni, P., Barbero, L., Bopp, L., Chevallier, F., Chini, L.P., Ciais, P., Currie, K., Delire, C., Doney, S.C., Friedlingstein, P., Gkritzalis, T., Harris, I., Hauck, J., Haverd, V., Hoppema, M., Goldewijk, K.K., Jain, A.K., Kato, E., Körtzinger, A., Landschützer, P., Lefèvre, N., Lenton, A., Lienert, S., Lombardozzi, D., Melton, J.R., Metzl, N., Millero, F., Monteiro, P.M.S., Munro, D.R., Nabel, J.E.M.S., Nakaoka, S.-I., Brien, K.O.A.A., Olsen, A., Omar, A.M., Ono, T., Pierrot, D., Poulter, B., Rödenbeck, C., Salisbury, J., Schuster, U., Schwinger, J., Séférian, R., Skjelvan, I., Stocker, B.D., Sutton, A.J., Takahashi, T., Tian, H., Tilbrook, B., van der Laan-Luijkx, I.T., van der Werf, G.R., Viovy, N., Walker, A.P., Wiltshire, A.J., Zaehle, S., 2016. Global carbon budget 2016. Earth Sys. Sci. Data 8:605–649. https://doi.org/10.5194/essd-8-605-2016.

Levin, I., Schuchard, J., Kromer, B., Münnich, K.O., 1989. The continental European Suess effect. Radiocarbon 31:431–440. https://doi.org/10.1017/s0033822200012017.

Lin, Y.L., Farley, R.D., Orville, H.D., 1983. Bulk parameterization of the snow field in a cloud model. J. Clim. Appl. Meteorol. 22:1065–1092. https://doi.org/10.1175/1520-0450(1983)022<1065:bpotsf>2.0.co;2.

Liu, Z., Guan, D., Wei, W., Davis, S.J., Ciais, P., Bai, J., Peng, S., Zhang, Q., Hubacek, K., Marland, G., Andres, R.J., Crawford-Brown, D., Lin, J., Zhao, H., Hong, C., Boden, T.A., Feng, K., Peters, G.P., Xi, F., Liu, J., Li, Y., Zhao, Y., Zeng, N., He, K., 2015. Reduced carbon emission estimates from fossil fuel combustion and cement production in China. Nature 524:335–338. https://doi.org/10.1038/nature14677.

Liu, Y., Gruber, N., Brunner, D., 2017. Spatiotemporal patterns of the fossil-fuel CO2 signal in central Europe: results from a high-resolution atmospheric transport model. Atmos. Chem. Phys. 17:14145–14169. https://doi.org/10.5194/acp-17-14145-2017.

Marland, G., Hamal, K., Jonas, M., 2009. How uncertain are estimates of CO2 emissions? J. Ind. Ecol. 13:4–7. https://doi.org/10.1111/j.1530-9290.2009.00108.x.

Miller, J.B., Lehman, S.J., Montzka, S.A., Sweeney, C., Miller, B.R., Karion, A., Wolak, C., Dlugokencky, E.J., Southon, J., Turnbull, J.C., Tans, P.P., 2012. Linking emissions of fossil fuel CO2 and other anthropogenic trace gases using atmospheric14CO2. J. Geophys. Res. 117, D08302. https://doi.org/10.1029/2011jd017048.

Niu, Z., Zhou, W., Cheng, P., Wu, S., Lu, X., Xiong, X., Du, H., Fu, Y., 2016a. Observations of atmospheric Δ14CO2 at the global and regional background sites in China: implication for fossil fuel CO2 inputs. Environ. Sci. Technol. 50:12122–12128. https://doi.org/10.1021/acs.est.6b02814.

Niu, Z., Zhou, W., Wu, S., Cheng, P., Lu, X., Xiong, X., Du, H., Fu, Y., Wang, G., 2016b. Atmospheric fossil fuel CO2 traced by Δ14C in Beijing and Xiamen, China: temporal variations, inland/coastal differences and influencing factors. Environ. Sci. Technol. 50:5474–5480. https://doi.org/10.1021/acs.est.5b02591.

Rivier, L., Ciais, P., Hauglustaine, D.A., Bakwin, P., Bousquet, P., Peylin, P., Klonecki, A., 2006. Evaluation of SF6, C2Cl4, and CO to approximate fossil fuel CO2in the northern hemisphere using a chemistry transport model. J. Geophys. Res. 111:D16311–15. https://doi.org/10.1029/2005jd006725.

Stocker, T.F., Qin, D., Plattner, G.K., Alexander, L.V., Allen, S.K., Bindoff, N.L., Bréon, F.M., Church, J.A., Cubasch, U., Emori, S., Forster, P., Friedlingstein, P., Gillett, N., Gregory, J.M., Hartmann, D.L., Jansen, E., Kirtman, B., Knutti, R., Kumar, K.K., Lemke, P., Marotzke, J., Masson-Delmotte, V., Meehl, G.A., Mokhov, I.I., Piao, S., Ramaswamy, V., Randall, D., Rhein, M., Rojas, M., Sabine, C., Shindell, D., Talley, L.D., Vaughan, D.G., Xie, S.P., 2013. Technical summary. Climate Change 2013: The Physical Science Basis. Contribution of Working Group I to the Fifth Assessment Report of the Intergovernmental Panel on Climate Change. Climate Change 2013 - The Physical Science Basis, Cambridge, United Kingdom and New York, NY, USA https://doi.org/10.1017/cbo9781107415324.005.

Stuiver, M., Polach, H.A., 1977. Discussion reporting of 14C data. Radiocarbon 19:355–363. https://doi.org/10.1017/s0033822200003672.

Turnbull, J.C., Miller, J.B., Lehman, S.J., Tans, P.P., Sparks, R.J., Southon, J., 2006. Comparison of 14CO2, CO, and SF6 as tracers for recently added fossil fuel CO2 in the atmosphere and implications for biological CO2 exchange. Geophys. Res. Lett. 33:1–5. https://doi.org/10.1029/2005gl024213.

Turnbull, J., Rayner, P., Miller, J., Naegler, T., Ciais, P., Cozic, A., 2009. On the use of $^{14}CO_2$ as a tracer for fossil fuel CO_2: quantifying uncertainties using an atmospheric transport model. J. Geophys. Res. 114:D22302–13. https://doi.org/10.1029/2009JD012308.

Turnbull, J.C., Keller, E.D., Norris, M.W., Wiltshire, R.M., 2016. Independent evaluation of point source fossil fuel CO2 emissions to better than 10%. Proc. Natl. Acad. Sci. U. S. A. 113:10287–10291. https://doi.org/10.1073/pnas.1602824113.

Wang, J., Wang, E., Yin, H., Feng, L., Zhang, J., 2014. Declining yield potential and shrinking yield gaps of maize in the North China plain. Agric. For. Meteorol. 195-196:89–101. https://doi.org/10.1016/j.agrformet.2014.05.004.

Wesely, M.L., 1989. Parameterization of surface resistances to gaseous dry deposition in regional-scale numerical models. Atmos. Environ. 23 (1967):1293–1304. https://doi.org/10.1016/0004-6981(89)90153-4.

Zhang, Q., Streets, D.G., Carmichael, G.R., 2009. Asian emissions in 2006 for the NASA INTEX-B mission. Atmos. Chem. Phys. 9:5131–5153. https://doi.org/10.5194/acp-9-5131-2009.

Zhou, W., Wu, S., Huo, W., Xiong, X., Cheng, P., Lu, X., Niu, Z., 2014. Tracing fossil fuel CO_2 using $\Delta^{14}C$ in Xi'an City, China. Atmos. Environ. 94:538–545. https://doi.org/10.1016/j.atmosenv.2014.05.058.